Processing and Application of Ceramics 11 [4] (2017) 235–246
https://doi.org/10.2298/PAC1704235S

Porous (Ba,Sr)TiO_3 ceramics for tailoring dielectric and tunability properties: Modelling and experiment

Roxana E. Stanculescu[1], Nadejda Horchidan[1], Carmen Galassi[2], Mihai Asandulesa[3], Leontin Padurariu[1,*], Cristina E. Ciomaga[4,*], Liliana Mitoseriu[1,*]

[1]*Dielectrics, Ferroelectrics & Multiferroics Group, Department of Physics, Al. I. Cuza Univ. of Iasi, 11 Carol I Bv., 700506, Iasi, Romania*
[2]*CNR -ISTEC, Via Granarolo no. 64, I-48018 Faenza, Italy*
[3]*Petru Poni Inst Macromol Chem, Grigore Ghica Voda Alley 41-A, Iasi 700487, Romania*
[4]*Research Department, Faculty of Physics, Dielectrics, Ferroelectrics & Multiferroics Group, Al. I. Cuza Univ. of Iasi, 11 Carol I Bv., 700506, Iasi, Romania*

Received 6 August 2017; Received in revised form 26 September 2017; Accepted 18 October 2017

Abstract

3D Finite Element Method simulations were employed in order to describe tunability properties in anisotropic porous paraelectric structures. The simulations predicted that properties of a ceramic can be tailored by using various levels of porosity. Porous $Ba_{0.6}Sr_{0.4}TiO_3$ (BST) ceramics have been studied in order to investigate the influence of porosity on their functional properties. The BST ceramics with various porosity levels have been obtained by solid-state reaction. Lamellar graphite in different concentration of 10, 20 and 35 vol.% was added as sacrificial pore forming agent. The structural, microstructural, dielectric and tunability properties were investigated. By comparison with dense BST ceramic, porous samples present a fracture mode transformation from intragranular to an intergranular fracture and a decrease of grain size. Lower dielectric constants, low dielectric losses, but higher values of tunability than in the dense material were obtained in the porous BST structures as a result of local field inhomogeneity generated by the presence of air pores-ceramic interfaces.

Keywords: *porous ceramic, solid state synthesis, ferroelectric properties, tunability, Finite Element Method*

I. Introduction

Ferroelectric oxides have been intensively studied in the past fifty years due to their wide range of application in electronic industry [1,2]. Permittivity in the range of hundreds and low losses are required for their use in microwave tunable devices, together with high dielectric nonlinearity (tunability). Since the high relative permittivity of barium titanate (BT) based ceramics limits the number of its applications, the need to adjust this value for such type of application requirements appeared. It was possible to discover countless compositions that fulfil the most appropriate technological requirements by doping and forming solid solutions or composites based on non-toxic BT [3,4]. Therefore, the macroscopic properties of such materials can be tailored to meet specific requirements that are essential for microwave application, such as thermal stability, lack of hysteresis, tunability above 1.5, permittivity below 1000, and dielectric losses <3% [5]. Methods to decrease the value of relative permittivity in ferroelectric-based ceramics were reported, like doping with extraneous ions [6,7], "dilution" by using low permittivity dielectrics in composites [8–10] or by decreasing the grain size down to nanoscale [11–13]. However, the moderate permittivity in such approaches is usually accompanied by a reduction of tunability.

A solution to reduce the hysteretic behaviour in ferroelectric materials is to form solid solutions. For example, in barium strontium titanate ($Ba_{1-x}Sr_xTiO_3$ (BST)) the functional properties can be tailored by controlling the substitution degree [3]. The molar fraction of

*Corresponding authors: tel: +40 232201102 (int. 2406),
e-mail: *cristina.ciomaga@uaic.ro* (Cristina Ciomaga)
leontin.padurariu@uaic.ro (Leontin Padurariu)
lmtsr@uaic.ro (Liliana Mitoseriu)

Sr influences the dielectric and ferroelectric properties of BST by modifying the temperature corresponding to the cubic-tetragonal phase transition and hence, its tetragonality. The composition $Ba_{0.6}Sr_{0.4}TiO_3$, which is in paraelectric cubic phase above 0 °C, is the prototype material for tunability application. Although DC-tunability values obtained in the ferroelectric state can be much higher than those obtained in the paraelectric one, the low losses and lack of hysteresis ensure a good reproductibility at high electric fields making the paraelectric state of such compounds more appealing for tunable applications [5,14,15]. Furthermore, this composition has attracted attention due to its potential for energy storage [16,17]. The disadvantage of this composition is the high values of the permittivity and losses at room temperature, due to proximity of the phase transition.

A complementary way to tailor the functional properties in ferroelectric-based ceramics is to use porosity in specially designed microstructures. Porosity strongly influences the dielectric properties by creating complex microscopic field frameworks according to the amount, shape and size of the pores. For many electroceramic applications the inevitable porosity generated in almost any kind of sintering is considered a disservice. However, it was recently demonstrated, both experimentally and theoretically, that porosity brings several advantages in some specific cases [18–22].

Porous materials can be considered as composites, consisting of a solid ceramic matrix with air pores filler. Recently, we have investigated the tunability properties in paraelectric-dielectric composites by 3D Finite Element Method (FEM) on the basis of Landau-Devonshire (LD) theory [23]. In this study, it was theoretically shown that for a paraelectric - linear dielectric composite (with equivalent amount of the phases), the highest tunability values and the lowest effective permittivity may be obtained when the relative permittivity of the filler phase is equal to 1. These results of FEM simulation showed that, among all the possible combinations between ferroelectrics and linear dielectrics, porous materials seem to be the most promising because their tunability is comparable with the one obtained in dense paraelectric structure. However, the porous structure proposed by Padurariu *et al.* [23] characterized by a porosity of 50% is on the limit of the mechanical stability and might be considered unrealistic for tunable properties. In spite of such a high porosity level, its effective permittivity was reduced only three times with respect to the dense composition. It is worth to mention that the model system proposed by Padurariu *et al.* [23] had a random distribution of the paraelectric/air phases without any anisotropy effects. Therefore, motivated by previous results, the new challenge was to explore new porous paraelectric systems with peculiar microstructures in the search for improved tunability properties, lower permittivity values at lower porosity levels and reduced dielectric loss.

II. Theoretical prediction by FEM

The most efficient way to decrease the effective permittivity in ferroelectric-linear dielectric composites is to create layered structures (2-2 connectivity) because a high electric field concentration is concentrated on the low permittivity dielectric layers (ε ~1–100), while the nonlinear high permittivity layers (ε ~100–1000) are subjected to very low fields. The concentration of high field on the dielectric layers in such structures explains why the effective permittivity is closer to the permittivity of the linear dielectric component. Another important advantage of this type of microstructure is that the dielectric loss is significantly reduced. Unfortunately, the same electric field configuration is responsible for rather low tunability values in layered composites, because the active ferroelectric/paraelectric component is subjected to very low fields where the non-linear character is almost undetectable [24,25]. On the other hand, Effective Medium Calculations or FEM simulations predicted relatively large tunability values in other types of microstructures like 0-3 (e.g. linear dielectric inclusions in a ferroelectric matrix) or randomly distributed phases [23–25]. In these systems some regions of the non-linear component are subjected to high enough local fields to generate an important level of permittivity non-linearity. Similar regions were also observed in ferroelectric thick films with mesoscopic holes by Whyte *et al.* and were called "hot spots" [26].

Using these observations, it seems reasonable to design new microstructures with 2-2-like connectivity in order to reach improved tunability properties, if the formation of such "hot spots" is allowed. Anisotropic porous structures with ellipsoidal pores are close to such a 2-2-like microstructure if the length of pores is much higher than their thickness and the pores are elongated in the direction perpendicular to the applied field (parallel to the electrodes). Such a microstructure with porosity of 35% and ratio between the length and the thickness of the pores of 5 is represented in Fig. 1a. This microstructure was computationally created by generating pores randomly distributed in the volume. The system represented in Fig. 1a is a parallel-plate capacitor with electrodes located on the top and the bottom surfaces. The local electric field within this system was calculated by 3D FEM using a procedure described in detail by Padurariu *et al.* [23]. In this procedure, the Laplace equation ($\nabla \cdot (\varepsilon \nabla V) = 0$, where V is the local potential) was solved considering two values for the local permittivity: 5000 for the paraelectric component (wine colour in Fig. 1a) and unity for air pores (grey colour in Fig. 1a). The corresponding local field image of the system from Fig. 1a is represented in Fig. 1b in colour scale. The local fields are highly inhomogeneous with a high concentration along the pores and lower average values on the dense paraelectric component. However, the appearance of some "hot spots" is noticeable in few regions in the paraelectric phase. These "hot spots" are

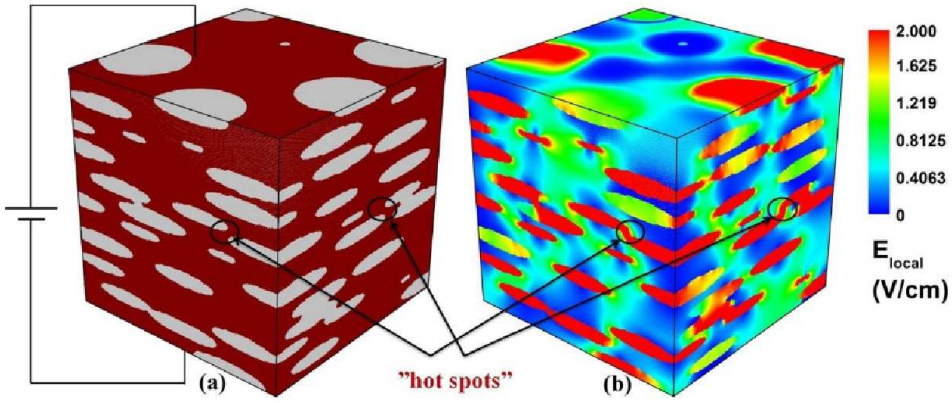

Figure 1. Anisotropic porous structure with 35% porosity (a) and the corresponding local field image simulated for the applied electric field of 1 V/cm (b)

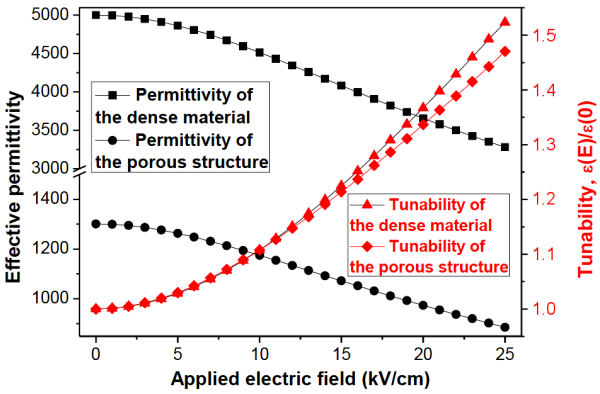

Figure 2. Dependences of the effective permittivity and tunability on the applied electric field for the dense paraelectric material and anisotropic porous structure represented in Figure 1

very important in such composites because their presence can contribute to the systems high tunability properties, as it will be shown later on.

In the next step, the dependence of the effective permittivity on the applied electric field was calculated according to the FEM-LD procedure, proposed by Padurariu *et al.* [23]. The tunability of the dense paraelectric material was set to 1.52 at an applied electric field of 25 kV/cm. The dependences of the effective permittivity and tunability on the applied electric field for the dense structure (used as input in FEM-LD calculations) and the porous structure are represented in Fig. 2. The simulation shows that the major impact of the anisotropic porosity is on the effective permittivity whose value decreases four times for a porosity of 35%. Tunability, on the other hand, presents only a slight decrease from 1.52 to 1.48, which confirms the key role of "hot spots" in such microstructures, as mentioned before.

These simulations predict that anisotropic porous paraelectric materials (2-2 like connectivity) might present interesting tunability properties. Therefore, a deeper experimental analysis on such kind of material deserves to be performed. The materials chosen for the investigation in this work are porous $Ba_{0.6}Sr_{0.4}TiO_3$ materials with various levels of porosity in the range from 4% to 32%.

III. Experimental methods

Titanium oxide (TiO_2 - 99.5% purity, Degussa P25), barium carbonate ($BaCO_3$ with purity >99%, Merck) and strontium carbonate ($SrCO_3$ with 99.9% purity, Aldrich) powders were weighed for the desired stoichiometry, then milled and calcined [21] in order to induce the formation of BST according to the reaction:

$$0.6BaCO_3 + 0.4SrCO_3 + TiO_2 \longrightarrow Ba_{0.6}Sr_{0.4}TiO_3 + CO_2\uparrow$$

Thereafter, the BST calcined powders were milled (Fig. 3, I) and mixed in proportions of 0 (BST0), 10 (BST10), 20 (BST20), and 35 vol.% (BST35) with fine grained graphite powder (Fig. 3, II) used as pore forming media. The mixed powders were uniaxially pressed (Fig. 3, III) in a stainless steel cylindrical die (30 mm inner diameter) by applying various pressures, as following: 50 MPa for pure BST powders and BST10, 40 MPa for BST20 and BST35, respectively. In order to obtain higher density for producing a dense reference sample, the green composition (BST0) was then cold-isostatic pressed at 300 MPa. The sintering treatment (Fig. 3, IV) was carried out at 1470 °C/2 h, with different heating steps, in order to facilitate releasing gases from the graphite burning process. Therefore, for the green compact with the highest graphite content a heating step of 100 °C/h was set, while for the others one of 150 °C/h was used. All the samples were placed on top of Al_2O_3 substrates and placed inside of a covered Al_2O_3 box to avoid the reaction of barium oxide with the crucibles. The resulting sintered ceramics with the perovskite ABO_3 structure complied with the formula $Ba_{0.6}Sr_{0.4}TiO_3$ were afterwards heated at 1100 °C/36 h and slowly cooled down to room temperature to allow the full re-oxidation process.

Bulk density of the sintered ceramic samples was measured by Archimedes method using a density analytical balance. Further, the ceramics were prepared for

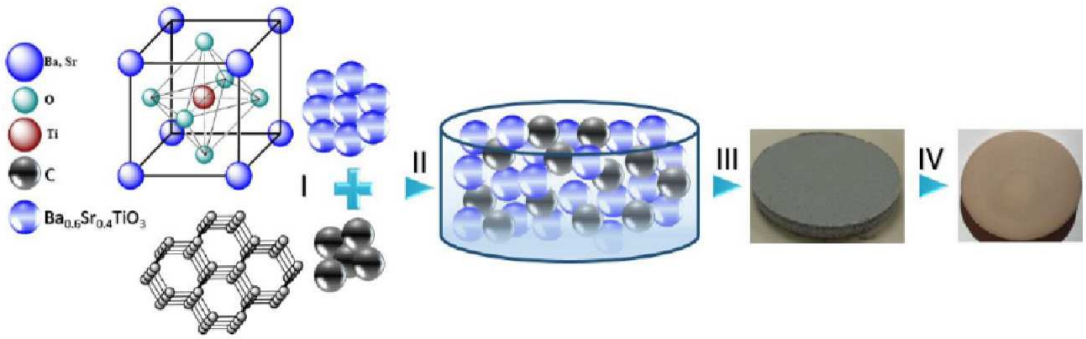

Figure 3. Preparation scheme in four steps for BST ceramics with variable porosity levels

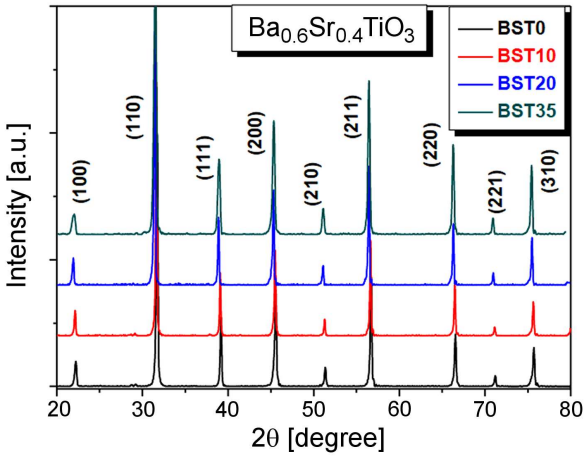

Figure 4. X-ray diffraction patterns of $Ba_{0.6}Sr_{0.4}TiO_3$ ceramics with different porosity levels

measurements of low and high field dielectric properties by applying silver paste electrodes (Pd-Ag) onto their plan-parallel surfaces.

The phase purity was checked with a Shimadzu XRD 6000 diffractometer by using Ni-filtered CuKα radiation (λ = 1.5418Å) with scan step increments of 0.02° and counting time of 1 s/step, for 2θ range between 20–80°. The microstructural aspects were investigated by scanning electron microscopy (SEM) measurements using FEI Quanta 200 variable pressure-environmental/ESEM. The low field dielectric properties were determined from measurements carried out in the frequency range of 20–10^6 Hz and temperature interval of −50–150°C using a dielectric spectrometer Concept 40 Novocontrol Technologies. The DC-tunability measurements were performed by placing the ceramic samples in a cell containing transformer oil using the circuit described in detail by Tufescu *et al.* [27]. A High-Voltage Amplifier Trek amplifier 30/20A-H-CE coupled with a function generator was set to deliver the high voltage. The experimental $P(E)$ loops were recorded by using a modified Sawyer-Tower circuit fed by a sinusoidal waveform with frequency of f = 10^5 Hz produced by a function generator Stanford Research Systems DS345 coupled with a High-Voltage Amplifier Trek 30/20A-H-CE.

IV. Results and discussion

4.1. Structural and microstructural characterization

The X-ray diffraction patterns recorded at room temperature are shown in Fig. 4. For all BST ceramic samples with different degrees of porosity, no obvious secondary phases can be observed and the split of (200) peaks corresponding to the tetragonality was not present, confirming that all the samples are in their paraelectric phase with cubic perovskite structure. It can be noticed that the intensity of (100) peak is reduced when increasing porosity, and the (200) and (210) peaks are enhanced (Fig. 4). This revealed the fact that the ceramics developed a preferential orientation of grain growth when increasing porosity, which may be attributed to the stress relaxation by the pores [28]. The (200) peak presents a shift with increasing porosity indicating slight modifications of unit cell parameters induced by the stress relaxation of crystalline lattice.

SEM images from Figs. 5a-d reflect the heterogeneous microstructural characteristics for BST ceramic samples with gradual increasing of porosity, as compared with the dense material. The microstructural analysis has revealed that the porosity induces disturbance in the BST system which is highlighted by the lower grain growth rate and the formation of randomly distributed and oriented intergranular pores.

Density measured after sintering for sample without graphite addition (BST0, Fig. 5a) was found to be near 96%. While for this sample the pores originated from the difference of diffusion rates between the barium and strontium species, in all the other cases (BST10, BST20 and BST35) the main contribution is derived from the pore forming media. Thus, porosity values for the samples with graphite content were measured as follows: 10% for BST10, 24% for BST20, and 32% for BST35. Graphite particles have a tendency to accumulate in high concentrations and to form clusters, which will affect the pores' size and shape, the homogeneity of pore distribution inside ceramics (BST10, Fig. 5b) but also the local composition inhomogeneity. The sintering conditions were chosen to permit the elimination of gasses resulting from the burnout of the graphite before closing the pores, in order to avoid the appearance of cracks

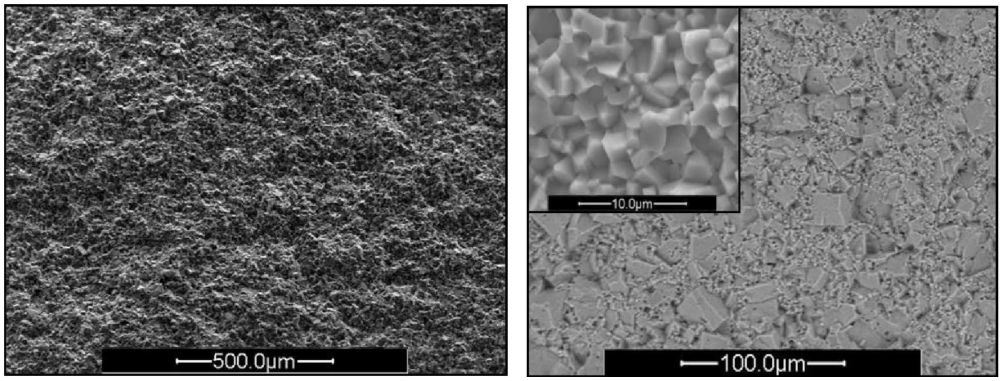

(a)

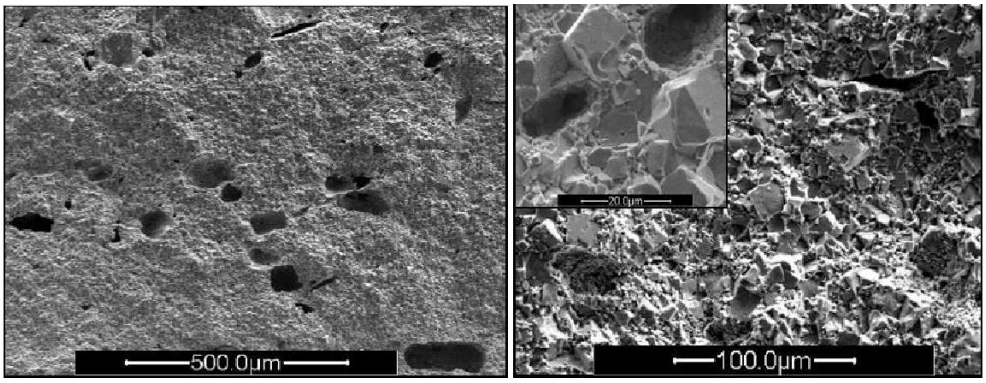

(b)

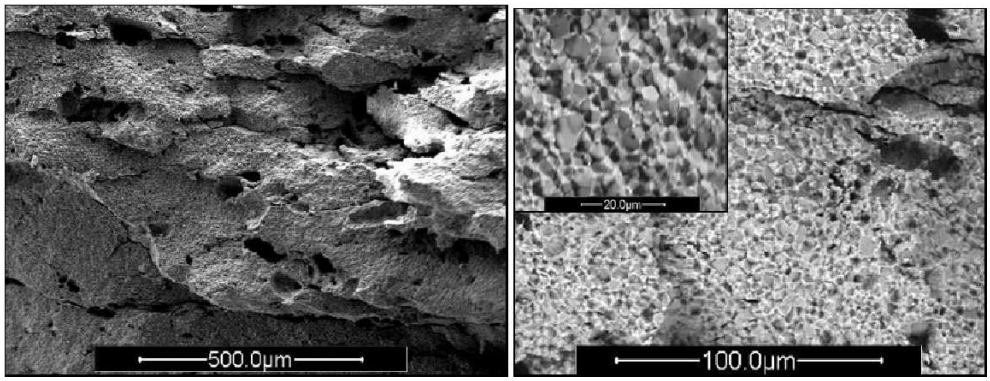

(c)

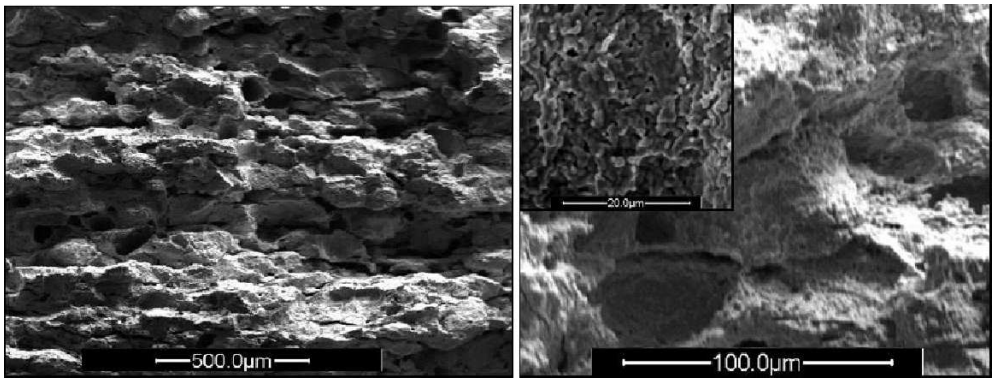

(d)

Figure 5. SEM microstructures of $Ba_{0.6}Sr_{0.4}TiO_3$ ceramic samples with progressive increase of porosity: a) dense BST0, b) BST with 10 vol.% graphite - BST10, c) BST with 20 vol.% graphite - BST20 and d) BST with 35 vol.% graphite - BST35

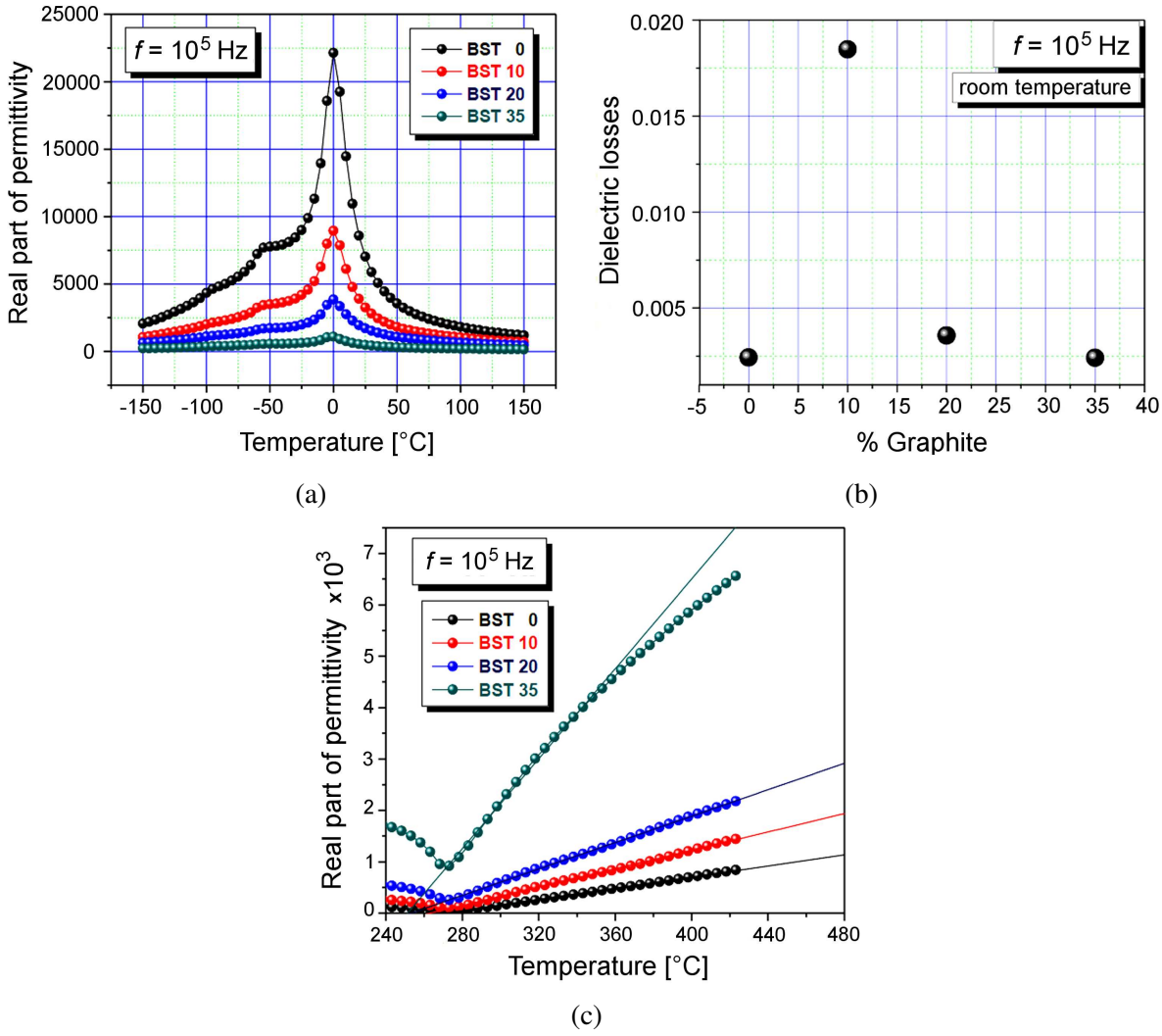

Figure 6. Relative dielectric permittivity *vs.* temperature measured at low electric fields for BST ceramics with various porosity levels (a), dependence of dielectric losses with graphite addition at room temperature (b), and Curie-Weiss analysis (c) (all dependences are presented for $f = 10^5$ Hz)

and mechanical failure in the final ceramic product. The pore forming media burns out and the gases evaporate. This is the moment when randomly distributed intergranular pores appear in the samples. The internal stress and strain of grains decrease, but close to pores it is magnified, so that the mobility of the domain walls is inhibited and grain boundaries are reduced. This is materialized as the inhibition of the grain growth. This process during the sintering begins with the amplification of stress and strain near the pores, which is a result of porosity [29].

Formation of multiple overlapping layers takes place when higher amounts of graphite are added to the BST system (BST20 and BST35, Fig. 5c,d). In these cases, the pores are present both in a layer plane and between layers, which emerge to intricate shapes and architectures. Both the grains and pores suffer significant changes. For the ceramics with higher addition of graphite, BST35, it can be observed that the pores are interconnected by separating ceramic layers due to the planar structure of graphite. Even though pores become larger and completely irregular, the grains appear smaller and rounded with an increased grain boundary interfaces (Fig. 5d).

Such peculiar microstructures, with complicated features and difficult to control, bring drastic influences on the macroscopic electrical properties of the material both at low and high fields.

4.2. Low and high field dielectric properties

Figure 6a depicts the temperature dependence of the relative permittivity at a given frequency $f = 10^5$ Hz for BST ceramics with different porosity levels. The evolution of dielectric losses with graphite addition at room temperature is presented in Fig. 6b. The Curie-Weiss analysis performed in the paraelectric state for all the samples is presented in Fig. 6c.

The low field dielectric properties can be discussed in two aspects: i) with respect to the phase transitions of $BaTiO_3$ and ii) by taking into account the effect of porosity in these types of ceramics with the same composition. Barium titanate has the Curie

point near 120 °C [30] which can be shifted by substitutions, as for example with increasing content of Sr^{2+} ions that replace Ba^{2+} ions in the BST lattice. Compared with pure barium titanate, all the structural phase transitions are shifted to lower temperatures values in $Ba_{0.6}Sr_{0.4}TiO_3$ composition. In particular, the cubic-to-tetragonal (paraelectric-to-ferroelectric) phase transition is lowered down to 0 °C, the tetragonal-to-orthorhombic phase transition takes place near −55 °C compared to pure barium titanate (6–12 °C), while the orthorhombic to rhombohedral phase transition is shifted from (−92–−77 °C) to near −95 °C. The obtained values are consistent with ones found by other authors in similar compositions [5].

The effect of porosity is clearly observed in Fig. 6. The dense BST0 ceramics at room temperature and $f = 10^5$ Hz presents high permittivity value of $\varepsilon \sim 7000$ and a sharp maximum of 22000 in the proximity of the Curie point (Fig. 6a). The paraelectric state is described by the Curie-Weiss behaviour (Fig. 6c). As porosity increases, the overall permittivity in the entire range of temperatures is lowered and the structural phase transitions become less prominent. In particular, this permittivity decrease is very pronounced at the Curie point. The maximum permittivity values in the porous ceramics at the same frequency are $\varepsilon \sim 9000$ (~3200 at room temperature) for BST10, $\varepsilon \sim 3800$ (over 1700 at room temperature) for BST20 and $\varepsilon \sim 1000$ (~480 at room temperature) for BST35. These transitions are marked by smooth maxima in ceramics with higher porosity. From Figs. 6a,c it can be observed that porosity level does not affect the critical temperatures, but only the amplitude of the relative permittivity and sharpness of the phase transitions. This is a result of twofold effect: i) the progressive "dilution" of the active component, i.e. by the increased porosity levels, which play a major role and ii) a reduction of grain sizes when increasing porosity, as revealed by SEM images. For all the BST ceramics, the dielectric losses ($\tan\delta$) are less than 6% in the investigated temperature range, and less than 2% at room temperature (Fig. 6b). As noticed, slightly higher losses were observed for BST10, for which most probably the sintering strategy did not allow the complete burning of graphite before closing the pores and most probably, small amounts of residual graphite remained trapped inside the ceramic pores.

Linear regression analysis on the temperature dependence of the reciprocal permittivity allows the calculation of the Curie Constant C and Curie-Weiss temperature T_0 (Fig. 6c). The investigated BST ceramics satisfy the Curie-Weiss law in the paraelectric region (only BST35 shows some deviations at higher temperatures), and the results are listed in Table 1.

Table 1. Curie constants calculated for all BST ceramic samples

Sample	f [kHz]	Curie constant	T_0 [K]	T_0 [°C]
BST0	350	1.8×10^5	272	0
BST10		1×10^5	265	−8
BST20		0.7×10^5	249	−25
BST30		0.2×10^5	254	−19

When porosity increases, the ferroelectricity strength decreases due to the progressive reduction of the polar phase amount, as indicated by the decrease of Curie constant, which is proportional to $\sim np^2$, where n is the volume dipole density and p is the individual dipolar moment. Although the Curie point is the same irrespective of porosity, which confirms that the intrinsic nature of the dense component is the same, the Curie-Weiss temperature T_0 diminishes when increasing porosity as a result of the progressive reduction of the active paraelectric phase amount.

The microstructural characteristics of the BST ceramic samples explain the low-field dielectric properties. There is a clear relationship between relative permittivity which is diminishing as a consequence of pores and layered-like microstructure, phase interconnectivity and the graphite addition.

The complex modulus formalism provides an additional tool for the analysis of material's electrical response, giving useful information concerning the charge transport mechanism. This analysis is based on polarization mechanisms and it was performed starting from the frequency dependence of the imaginary part of dielectric modulus at different temperatures [31]. The frequency dependence of the imaginary part of dielectric modulus for some temperatures is shown in Fig. 7a-d.

Dielectric relaxation phenomena are highlighted by peaks in the complex dielectric modulus *vs.* frequency, with maxima shifted to higher frequency when the temperature T increases. As it can be seen from Fig. 7, the relaxation rates of these processes increase with decreasing temperature and all the samples show this relaxation of M'' in the range of 10^2–10^5 Hz, with a similar trend. Among all the ceramics, only the BST10 with the lowest porosity has an additional relaxation phenomenon at higher frequencies, i.e. above 10^5 Hz which most probably has another cause (Fig. 7b).

A detailed insight into the activation and relaxation mechanisms, as well as conduction phenomena involved in the investigated porous BST ceramics, is useful for a better understanding of ceramics' physical nature. The complex modulus obeys the Arrhenius-type law according to equation:

$$f = f_0 \cdot \exp\frac{-E_a}{k \cdot T_m} \tag{1}$$

where f_0 is the pre-exponential term, k the Boltzmann constant, and T_m the temperature corresponding to the dielectric modulus maxima and E_a is the activation energy for the relaxation phenomenon. These calculations aim to determine the speed wherewith every peak corresponding to the different values of temperature shown in the imaginary part of dielectric modulus is shifted

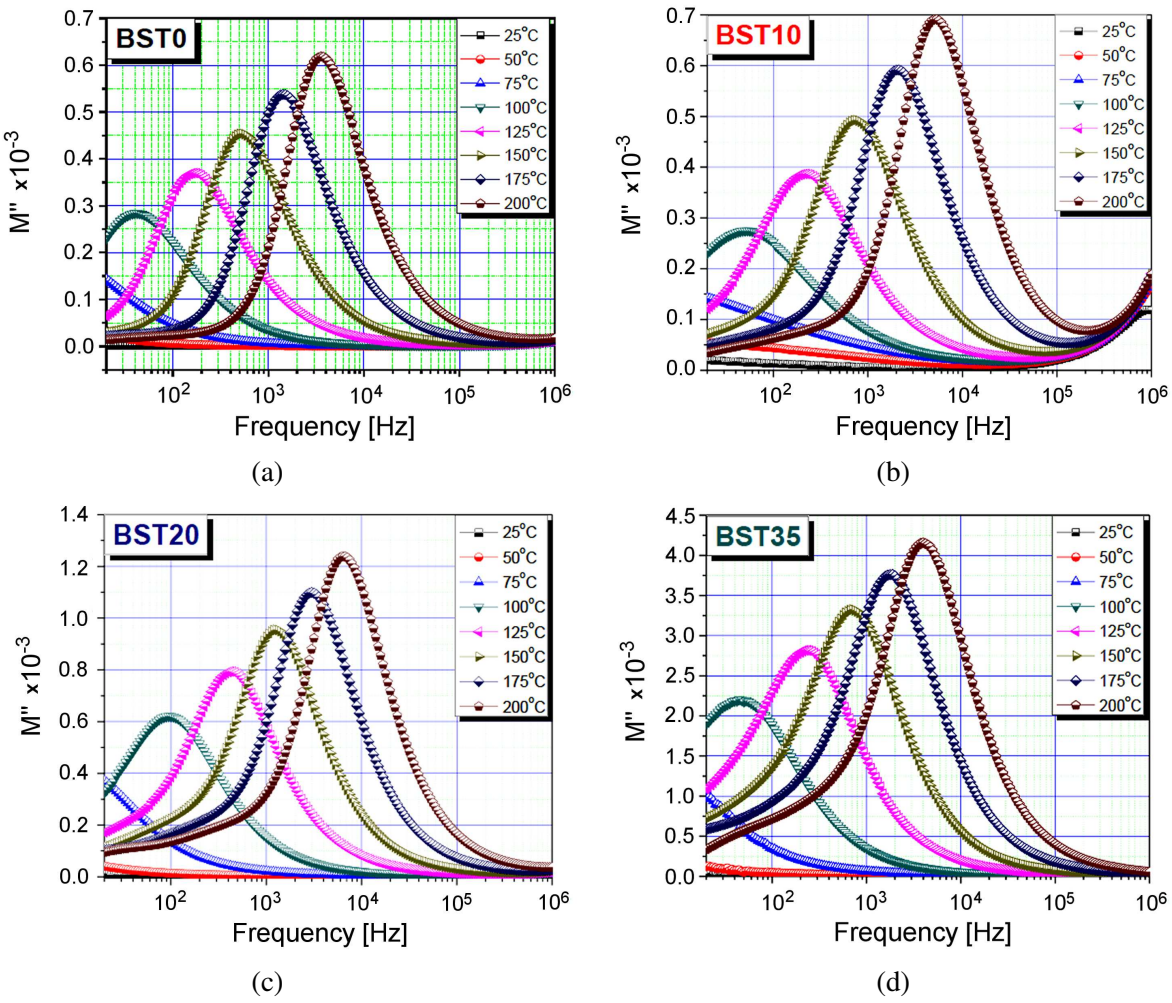

Figure 7. Representation of the imaginary part of dielectric modulus as a function of frequency for several temperatures for BST ceramic samples with different degrees of porosity

towards higher frequencies when temperature is increased (Fig. 7a–d). Such a continuous dispersion observed when frequency increases may be attributed to the short-range mobility of charge carriers and suggests a thermally activated dielectric relaxation process.

The results from Arrhenius calculations concerning the dielectric modulus for determining the activation energies and relaxation times involved in the dielectric response of BST ceramic samples with different degrees of porosity are shown in Table 2.

Two temperature ranges for the dielectric relaxations have been determined by the Arrhenius analysis: one between 90–120 °C characterized by activation energies in the range 0.78–0.87 eV and characteristic $\tau \sim 10^{-14}$–10^{-13} s and a faster process in the range of 120–200 °C, with slightly lower activation energies of 0.59–0.68 eV and relaxation times $\tau \sim 10^{-12}$–10^{-11} s. The determined values are quite similar, irrespective of porosity and this leads to the idea that they are mainly determined by charged defects present in the ceramic part of the samples. However, there is a tendency of increasing the activation energy when increasing porosity for the faster process. This can be related to the presence of a larger number of ceramic-air pores interfaces that might trap such charged defects.

Table 2. Curie constants calculated for all BST ceramic samples

Sample	BST0	BST10	BST20	BST35
f = 20–200 Hz, T = 90–120 °C				
E_a [eV]	0.78	0.79	0.87	0.85
τ [s]	11×10^{-14}	8×10^{-14}	0.35×10^{-14}	1.24×10^{-14}
f = 200–5000 Hz, T = 120–200 °C				
E_a [eV]	0.66	0.68	0.59	0.62
τ [s]	414×10^{-14}	177×10^{-14}	1279×10^{-14}	948×10^{-14}

For a better understanding of the observed dielectric behaviour, temperature dependence of relaxation time constant is discussed. The hopping mechanism of charge carriers intrinsically dominates in these relaxations and in perovskites they are often related to the oxygen deficiency. Activation energy values in the range of 0.3–0.5 eV have been reported in literature as arising from the oxygen vacancies in single ionized state, while those in the range of 0.6–1.2 eV are commonly associated to the double ionized oxygen vacancies [32–34]. The main charged defects in our ceramics might be

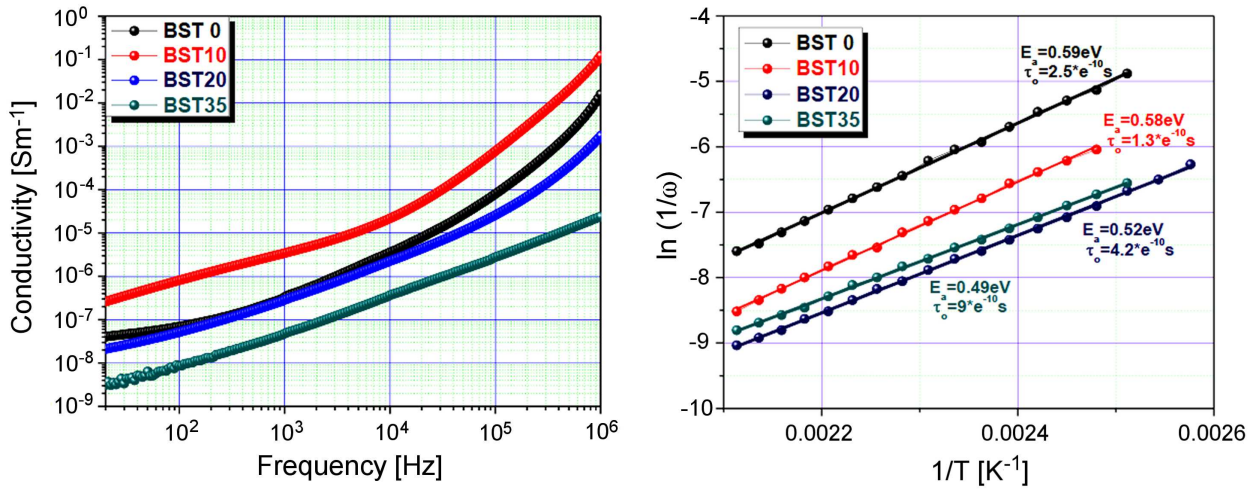

(a) (b)

Figure 8. Variation of conductivity *vs.* frequency (a) and the reciprocal of angular frequency dependence *vs.* reciprocal temperature in a representation based on conductivity (b) for determining the activation energies and relaxation time involved in the dielectric response of BST ceramic samples with different degrees of porosity

the above mentioned oxygen vacancies (single or double ionized) and the corresponding electrons released for electroneutrality as well as uncompensated charges at the ceramic-air pores interfaces $\sigma_{pol} = \vec{P} \cdot \vec{n}$ or in regions characterized by variation of polarization (ceramic grain boundaries): $\rho = -\mathrm{div}\vec{P}$ which usually produce thermally activated Maxwell Wagner interfacial relaxations. It is worth to mention that our samples have been re-oxidized in order to eliminate or at least to reduce the oxygen vacancies resulted from the presence of reducing atmosphere nearby the carbonaceous fillers. In spite of this, we do not exclude the possible remanence of some small amounts of oxygen vacancies in the ceramic volume, but their density might reduce with increasing porosity. In addition, higher values of activation energy suggest a lower concentration of space charges or vacancies in our samples or the presence of some additional relaxation phenomena of different origin.

In order to obtain more information concerning the electrical conduction mechanism in these BST ceramics, the AC-conductivity *vs.* frequency (Fig. 8a,b) was also analysed. The corresponding activation energies have been also determined. In Fig. 8b the calculated values for the activation energy are in the range of 0.5–0.6 eV, which are in the range of ones reported for oxygen vacancies in perovskites usually ascribed to the polarization of the space charge carriers or to the conduction phenomena in the grain boundaries inside the ceramic oxide [34]. As temperature increases, the investigated relaxation mechanisms are strongly related to the released concentration and recombined space charges which dominate the ionic conductivity mainly attributed to the grain boundary effect of the dense areas in the BST ceramics.

It is worth to note that low-frequency conductivity is in the range of 10^{-9}–10^{-7} S m^{-1} (Fig. 8 a) and still decreases towards a lower DC conductivity (*i.e.* the σ_{DC} plateau was not reached yet at decreasing frequency). The highest conductivity is observed in the BST10 sample for which a new relaxation mechanism was found at high frequencies (fast response). One may relate this behaviour to the possible residuals of carbon black inside the pores in this particular composition. Very good dielectric characteristics of the porous samples make the application of high electric fields possible.

The effect of different microstructures at room temperature tunability has been determined *via* high field dielectric measurements. The evolution of permittivity as a function of DC electric field is shown in Fig. 9a up to the maximum field of 2.2 kV/mm. The relative tunability is shown in Fig. 9b.

Irrespective of porosity level, the typical permittivity dependence as a function of the applied electric field was corresponding to the paraelectric behaviour at room temperature in BST compositions, with a lack of hysteresis and nonlinear but non-saturated $\varepsilon(E)$ dependence up to the maximum applied field. As it can be seen from the Fig. 9a, at zero field, the dense BST0 ceramic presents the highest value of dielectric permittivity that reduces from 9200 down to 6500 with application of a DC electric field up to 2.2 kV/mm (corresponding to the tunability of ~1.41). With increasing porosity, the permittivity strongly decreases down to ~480 for 32% porosity (BST35), ~1800 for 24% (BST20) and ~3350 for 10% (BST10). In spite of lowering the amount of the active phase when increasing porosity, the tunability is preserved at high values, like in the dense structure, for all the porous ceramics, as predicted by FEM calculations. It is very interesting that in the sample with the highest porosity (BST35), a strong decrease of the effective permittivity of 95% was accompanied with the tunability maintained almost at the same level as in the dense material (reduction of only 6% is found). This re-

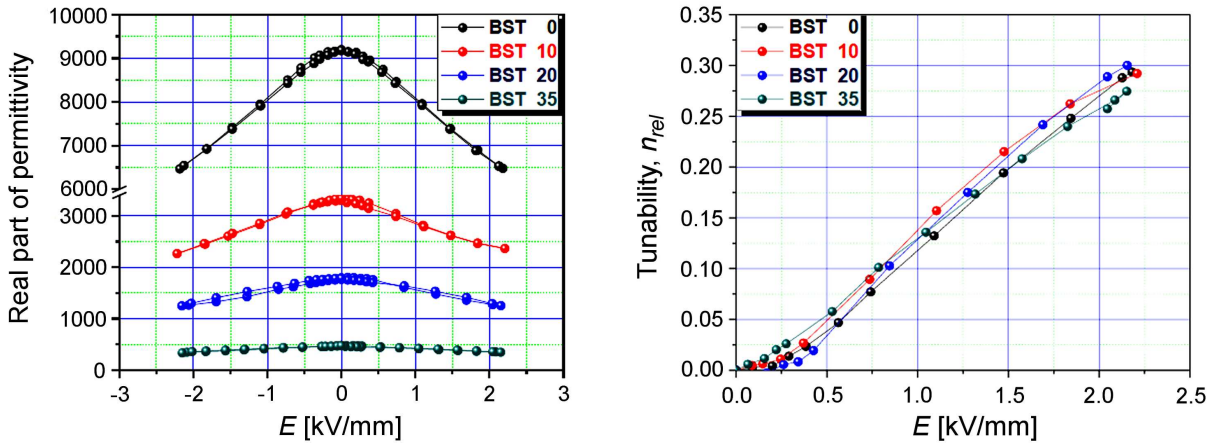

(a) (b)

Figure 9. The real part of permittivity dependence *vs.* DC electric field (a) and the corresponding relative tunability for the BST ceramics with various porosity levels (b)

sult is in an excellent agreement with the prediction of the FEM simulations.

To better characterize the porous samples also from the ferroelectric point of view, the $P(E)$ hysteresis loops were recorded at room temperature at the fixed applied electric field (Fig. 10). An enhanced electric field will be accompanied by a higher leakage current caused by the space charge effect [35,36]. For the maximum applied field, $P(E)$ loop for the dense BST0 sample is slim, with $P_r = 0.5\,\mu C/cm^2$ and $E_c < 0.1$ kV/mm. The coercive field slightly increases up to 0.2 kV/mm with increasing porosity value above 24% (BST20). Switching characteristics of BST35 ceramic are still noticed although remnant polarization is strongly diminished and coercive field increases above 0.4 kV/mm. The switching characteristics reflect the paraelectric behaviour of $Ba_{0.6}Sr_{0.4}TiO_3$ composition at room temperature, even though the $P(E)$ dependence is tilted and not completely linear. This is due to the remnant ferroelectric regions inside the sample above the Curie temperature and some

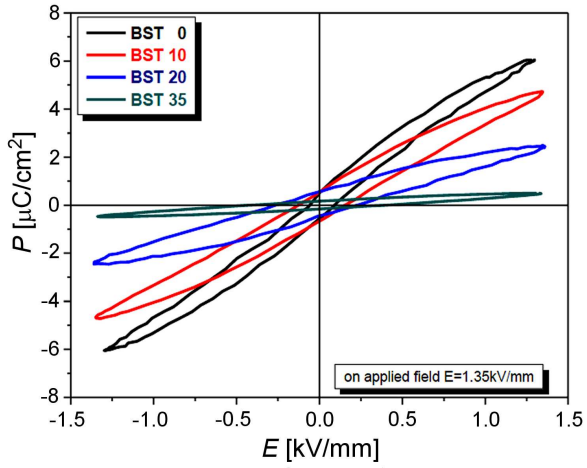

Figure 10. Room temperature *P(E)* hysteresis loops for BST ceramics with gradual decrease of density at 1.35 kV/mm applied electric field

conductivity losses activated at high fields. The maximum polarization together with the $P(E)$ slope ($\sim \varepsilon$) gradually reduces when increasing porosity and the hysteresis loop area sharply falls for samples with higher porosity.

When DC electric field is applied, the space charges are accumulated inside the pores and at the interfaces enclosed by the grain boundaries. Thus, a larger amount of spatial charges may be found in the fine grained regions of the sample. Pores can also share the DC bias field when they are interconnected. Due to the porosity of the samples, collective effects will be created and then a full polarization of porous samples is difficult to obtain due to the presence of a large leakage current arising from the pores.

V. Conclusions

3D FEM calculations predicted the possibility to reduce permittivity while maintaining a high level of tunability comparable to one obtained in the dense material in layered-like porous structures. Single phase $(Ba,Sr)TiO_3$ powders obtained via solid state reaction and variable amounts of graphite were used to prepare ceramic materials with various porosity levels and anisotropic elongated porosity. The sintered ceramics exhibited smaller grains and lower densification as graphite addition increased.

Porous $Ba_{0.6}Sr_{0.4}TiO_3$ compositions in the paraelectric state at room temperature show a strong temperature variation of the permittivity induced by the proximity of their phase transition. The dielectric measurements revealed high maximum permittivity values, over 1000 for BST35 and above 20000 for BST0. All ceramics show a well-defined ferro-para (tetragonal-cubic) phase transition at ~0 °C, followed by a Curie-Weiss behaviour and $\tan\delta$ below 6% at $f = 10^5$ Hz, in the temperature range of 25–200 °C. The Curie constant and polarization decreases with porosity increase as result of the "dilution" effect by increasing porosity.

The present study shows that even the zero field permittivity decreases up to 20 times with increasing the porosity level up to 35%. The relative DC-tunability of porous samples is kept at similar values as in the dense ceramics. The idea to design porous ferroelectric microstructures for tunable devices deserves additional consideration since the zero field permittivity may be tailored with the impact on the functional properties. The increasing amount of ferroelectric-air pore interfaces when decreasing ceramics density generate improved tunability properties which are most likely ascribed to the ability of these interfaces to concentrate the electric field in some regions ("hot spots").

Acknowledgements: This work was financially supported by CNCS-UEFISCDI project PN-II-RU-TE-2014-4-1494.

References

1. J.F. Scott, "Applications of modern ferroelectrics", *Science*, **315** [5814] (2007) 954–959.
2. G.H. Haertling, "Ferroelectric ceramics: History and technology", *J. Am. Ceram. Soc.*, **82** [4] (1999) 797–818.
3. L.P. Curecheriu, L. Mitoseriu, A. Ianculescu, "Nonlinear dielectric properties of $Ba_{1-x}Sr_xTiO_3$ ceramics", *J. Alloys Compd.*, **482** [1-2] (2009) 1–4.
4. N. Horchidan, A.C. Ianculescu, C.A. Vasilescu, M. Deluca, V. Musteata, H. Ursic, R. Frunza, B. Malic, L. Mitoseriu, "Multiscale study of ferroelectric-relaxor crossover in $BaSn_xTi_{1-x}O_3$ ceramics", *J. Eur. Ceram. Soc.*, **34** [15] (2014) 3661–3674.
5. A.K. Tagantsev, V.O. Sherman, K.F. Astafiev, J. Venkatesh, N. Setter, "Ferroelectric materials for microwave tunable applications", *J. Electroceram.*, **11** (2003) 5–66.
6. R. Laishrama, K.C. Singhb, C. Prakasha, "Enhanced dielectric loss of Mg doped $Ba_{0.7}Sr_{0.3}TiO_3$ ceramics", *Ceram. Int.*, **42** (2016) 14970–14975.
7. Q. Zhang, J. Zhai, Q. Ben, X. Yu, X. Yao, "Enhanced microwave dielectric properties of $Ba_{0.4}Sr_{0.6}TiO_3$ ceramics doping by metal Fe powders", *J. Appl. Phys.*, **112** [10] (2012) 104104.
8. G. Hu, F. Gao, L. Liu, B. Xu, Z. Liu, "Microstructure and dielectric properties of highly tunable $Ba_{0.6}Sr_{0.4}TiO_3$/MgO/Al_2O_3/ZnO composite", *J. Alloys Compd.*, **518** (2012) 44–50.
9. Q. Xue, H. Du, X. Gao, Y. Wang, Y. Zhang, J. Xu, G. Wang, Q. Ding, C. Tian, C. Liu, Y. Lü, S. Li, "The effect of MnO_2-doping on the microstructure and microwave dielectric properties of BST/MgO composites", *J. Alloys Compd.*, **615** (2014) 372–374.
10. Y. Wu, J.J. Bian, C. Zhao, S.J. Luo, "Improvement of dielectric loss of $Ba_{0.75}Sr_{0.25}TiO_3$ tunable material by $La_{0.5}Na_{0.5}TiO_3$ addition", *J. Mater. Sci.: Mater. Electron.*, **26** (2015) 90–97.
11. Q. Zhang, Zhai, B. Shen, H. Zhang, X. Yao, "Grain size effects on dielectric properties of barium strontium titanate composite ceramics", *Mater. Res. Bull.*, **48** (2013) 973–977.
12. L.P. Curecheriu, M.T. Buscaglia, V. Buscaglia, Z. Zhao, L. Mitoseriu, "Grain size effect on the nonlinear dielectric properties of barium titanate ceramics", *Appl. Phys. Lett.*, **97** [24] (2010) 2909.
13. L. Padurariu, L. Curecheriu, V. Buscaglia, L. Mitoseriu, "Field-dependent permittivity in nanostructured $BaTiO_3$ ceramics: Modeling and experimental verification", *Phys. Rev. B*, **85** (2012) 224111.
14. J. Wang, L. Tang, B. Shenn, J. Zhai, "Property optimization of BST-based composite glass ceramics for energy-storage applications", *Ceram. Int.*, **40** (2014) 2261–2266.
15. C. Liu, P. Liu, "Microstructure and dielectric properties of BST ceramics derived from high-energy ball-milling", *J. Alloys Compd.*, **584** (2014) 114–118.
16. Z. Song, H. Liu, S. Zhang, Z. Wang, Y. Shi, H. Hao, M. Cao, Z. Yao, Z. Yu, "Effect of grain size on the energy storage properties of $(Ba_{0.4}Sr_{0.6})TiO_3$ paraelectric ceramics", *J. Eur. Ceram. Soc.*, **34** (2014) 1209–1217.
17. B.B. Liu, X.H. Wang, R.X. Zhang, L.T. Li, "Energy storage properties of ultra-fine-grained $Ba_{0.4}Sr_{0.6}TiO_3$-based ceramics sintered at low temperature", *J. Alloys Compd.*, **691** (2017) 619–623.
18. Y. Zhang, G. Wang, T. Zeng, R. Liang, X. Dong, "Electric field-dependent dielectric properties and high tunability of porous $Ba_{0.5}Sr)0.5TiO_3$ ceramics", *J. Am. Ceram. Soc.*, **90** [4] (2007) 1327–1330.
19. Y. Zhang, G. Wang, K. Wang, Y. Wang, X. Dong, "The model of electric field dependent dielectric properties for porous ceramics", *J. Appl. Phys.*, **103** (2008) 114103.
20. L. Padurariu, L. Curecheriu, C. Galassi, L. Mitoseriu, "Tailoring non-linear dielectric properties by local field engineering in anisotropic porous ferroelectric structures", *Appl. Phys. Lett.*, **100** (2012) 252905.
21. R. Stanculescu, C.E. Ciomaga, L. Padurariu, P. Galizia, N. Horchidan, C. Capiani, C. Galassi, L. Mitoseriu, "Study of the role of porosity on the functional properties of $(Ba,Sr)TiO_3$ ceramics", *J. Alloys Compd.*, **643** (2015) 79–87.
22. L. Mitoseriu, L. Padurariu, Chapter 18 "Local field enginnering approach for tuning dielectric and ferroelectric properties in nanostructured ferroelectrics and composites", pp. 588–611 in *Nanoscale Ferroelectrics and Multiferroics Key Processing and Characterization Issues, and Nanoscale Effects*, Eds. M. Alguero, J. Marty Gregg, L. Mitoseriu. Wiley, UK, 2016.
23. L. Padurariu, L.P. Curecheriu, L. Mitoseriu, "Nonlinear dielectric properties of paraelectric-dielectric composites described by a 3D Finite Element Method based on Landau-Devonshire theory", *Acta Mater.*, **103** (2016) 724–734.
24. V.O. Sherman, A.K. Tagantsev, N. Setter, D. Iddles, T. Price, "Ferroelectric-dielectric tunable composites", *J. Appl. Phys.*, **99** (2006) 074104.
25. K.F. Astafiev, V.O. Sherman, A.K. Tagantsev, N. Setter, "Can the addition of a dielectric improve the figure of merit of a tunable material", *J. Eur. Ceram. Soc.*, **23** (2003) 2381–2386.
26. J.R. Whyte, R.G.P. McQuaid, P. Sharma, C. Canalias, J.F. Scott, A. Gruverman, J.M. Gregg, "Ferroelecric domain wall injection", *Adv. Mater.*, **26** (2014) 293–298.
27. F.M. Tufescu, L. Curecheriu, A. Ianculescu, C.E. Ciomaga, L. Mitoseriu, "High-voltage tunability measurements of the $BaZr_xTi_{1-x}O_3$ ferroelectric ceramics", *J. Optoelectron. Adv. Mater.*, **10** [7] (2008) 1894–1897.
28. C. Mao, S. Yan, S. Cao, C. Yao, F. Cao, G. Wang, X. Dong, X. Hu, C. Yang, "Effect of grain size on phase transition, dielectric and pyroelectric properties of BST ceramics", *J.*

Eur. Ceram. Soc., **34** (2014) 2933–2939.
29. T. Zeng, X.L. Dong, C.L. Mao, Z.Y. Zhou, H. Yang, "Effects of pore shape and porosity on the properties of porous PZT 95/5 ceramics", *J. Eur. Ceram. Soc.*, **27** (2007) 2025–2029.
30. M.G. Harwood, P. Popper, D.F. Rushman, "Curie point of barium titanate", *Nature*, **160** (1947) 58–59.
31. L. Curecheriu, P. Postolache, V. Buscaglia, N. Horchidan, M. Alexe, L. Mitoseriu, "$BaTiO_3$-ferrite composites with magnetocapacitance and hard/soft magnetic properties", *Phase Trans.*, **86** [7] (2013) 670–680.
32. S. Kang, S.K. Choi, C.H. Park, "Diffuse dielectric anomaly in perovskite-type ferroelectric oxides in the temperature range of 400-700 degrees C", *J. Appl. Phys.*, **94** (2003) 1904–1911.
33. C.E. Ciomaga, M.T. Buscaglia, V. Buscaglia, L. Mitoseriu, "Oxygen deficiency and grain boundary-related giant relaxation in $Ba(Zr,Ti)O_3$ ceramics", *J. Appl. Phys.*, **110** (2011) 114110.
34. Z. Lia, H. Fan, S. Jia, L.F. Song, J. Wang, "Dielectric relaxation at high temperatures induced by oxygen vacancies at grain boundary in Na-doped barium strontium titanium ceramics", *Solid State Ionics*, **269** (2015) 14–18.
35. I. Rivera, A. Kumar, N. Ortega, R.S. Katiyar, S. Lushnikov, "Divide line between relaxor, diffused ferroelectric, ferroelectric and dielectric", *Solid State Commun.*, **149** (2009) 172–176.
36. L. Jin, F. Li, S.J. Zhang. "Decoding the fingerprint of ferroelectric loops: comprehension of the material properties", *J. Am. Ceram. Soc.*, **97** (2014) 1–27.